Nano Research

Open Access

Research Article

# An optical carbon nanotube fibre probe for measurement of nano structures with large aspect ratio

Weihao Tao[1], Shuhao Zhao[1], Hanjin Dong[1], Ze Zhang[1], Peirui Ji[1], Shenghan Qin[1], Wenbo Hu[1], Jinlong Zhu[2], Renjie Zhou[3], and Shuming Yang[1] ✉

[1] State Key Laboratory for Manufacturing Systems Engineering, Xi'an Jiaotong University, Xi'an 710049, China
[2] State Key Laboratory of Intelligent Manufacturing Equipment and Technology, Huazhong University of Science and Technology, Wuhan 430074, China
[3] Department of Biomedical Engineering, The Chinese University of Hong Kong, Hong Kong, China

**Cite this article:** *Nano Research*, **2025**, *18*, 94907254. https://doi.org/10.26599/NR.2025.94907254

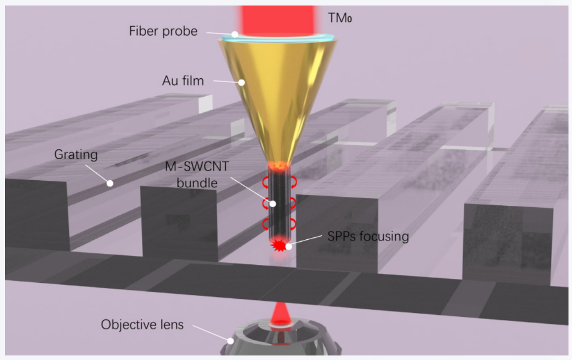


**ABSTRACT:** With the development of imaging and measurement technologies, scanning near-field optical microscopy (SNOM) has achieved high signal-to-noise ratio. The resolution of a fibre probe-based SNOM system is capable of reaching 10 nm. However, SNOM applications are presently constrained to the measurement of near-field optical information to relatively straightforward structures, including quantum dots, carbon nanotubes, graphene, and so forth. The geometry of conventional fibre probes, with tips at an angle of 30°–60°, presents a challenge for accurately imaging complex surface structures. This paper proposes a carbon nanotube composite fibre probe (CNT-FP) with a large aspect ratio. The key point is that a carbon nanotube bundle is composited at the tip of conventional surface plasmon polaritons fibre probes (SPPs-FP), which are the fibre probes coated with gold film to excite the SPPs. The coupling, propagation, and focusing effects of SPPs on the carbon nanotube bundle are verified. CNT-FPs have been fabricated and applied to measure a grating with the depth of 400 nm and the width of 400 nm. The experimental results show that the measurement accuracy and imaging quality of CNT-FP are nearly one order of magnitude higher than that of conventional SPPs-FP, as evidenced by evaluation criteria such as line roughness and volatility index. Moreover, it achieves an optical resolution of 72.1 nm in the measurements of a nano structure with large aspect ratio. It provides an effective solution of measuring structures with larger aspect ratios.

**KEYWORDS:** carbon nanotubes, fibre optic probes, surface plasmon polaritons, nano-focusing, large aspect ratio

## 1 Introduction

In recent years, with the introduction of the concept of surface plasmon polaritons (SPPs) [1, 2], scanning near-field optical microscopy (SNOM) and its probes have achieved significant improvement. By exciting SPPs in different ways, such as coating metallic film [3, 4], small hole diffraction [5–7], grating-coupling excitation [8, 9], and fibre-nanowire-coupling excitation [10, 11], we can compress and focus the optical field to the nanoscale, which greatly improves the signal strength and resolution [12]. However, SNOM applications are presently constrained to the measurement of near-field optical information to relatively straightforward structures with nearly zero aspect ratio, including quantum dots [13], carbon nanotubes [14, 15], graphene [16–18], and so forth. Normally, the near-field optical signal is only excited if the tip of the probe enters the near-field range above the sample, typically within 50 nm. When the measured structure has a large drop (more than tens of nanometres) in the vertical direction or has a large aspect ratio [19–21], compared to samples exhibiting near-zero aspect ratios, such as carbon nanotubes and quantum dots, structures with considerable aspect ratios are designated as large depth-to-width structures, conventional surface plasmon polaritons fibre probes (SPPs-FP) are unable to enter the near-field range above the sample due to the limitations of the geometries. Therefore, it is not feasible to collect near-field optical signals for each point, which in turn affects the accuracy of near-field optical imaging. In atomic force microscopy (AFM) applications, the use of a carbon nanotube compound at the tip of the AFM probe [22–24] allows for more

**Received:** November 28, 2024; **Revised:** January 12, 2025
**Accepted:** January 13, 2025

✉ Address correspondence to shuming.yang@mail.xjtu.edu.cn

accurate measurement of the topography of structures with large aspect ratios, such as deep grooves or holes. This technique enables deeper penetration into the bottom of the structure, thereby facilitating the restoration of the topography of the sample under test with greater precision. Analogously, for SNOM applications, one-dimensional nanomaterial extending from the tip of the probe can be used to conduct the SPPs to the tip of the one-dimensional nanomaterial [25], forming a focused light field deep into the depth of the structure with a larger aspect ratio, and achieving a more accurate imaging of the near-field optical signals. We have noted that attempts have been made to achieve more accurate near-field optical measurements using metallic nanowires, such as Ag nanowires [11, 26, 27]. Nevertheless, Ag nanowires are susceptible to oxidation in air, necessitating their utilization in a vacuum or inert gas environment. As a one-dimensional nanomaterial with extremely excellent electrical conductivity [28–30], metallic single-walled carbon nanotubes (m-SWCNT) [30, 31] can be used as an excellent carrier for the propagation of SPPs, and its ultra-high hardness and good flexibility can effectively improve the resistance to abrasion and extend the operation life of the probe. Compared to silver nanowires, m-SWCNTs are more chemically stable in air to be preserved for long periods of time [32]. In this paper, we use m-SWCNT which have excellent SPPs conductivity and more stable chemistry in the air to fabricate composite probes, so it enables higher quality scanning imaging of samples with large aspect ratios.

## 2 Results and discussion

In this paper, we demonstrate a carbon nanotube composite fibre probe (CNT-FP) with large aspect ratio for near-field optical microscopy applications, as shown in Fig. 1(a), which composites a metallic single-walled carbon nanotube bundle (m-SWCNTB) consisting of multiple m-SWCNTs at the tip of a conventional SPPs-FP to enable near-field optical measurements of complex surface structures with larger aspect ratios. We used a finite difference time domain (FDTD) approach to analytically validate the feasibility of CNT-FP for excitation, propagation, and focusing of SPPs. As shown in Fig. 1(b), under the incident light in transverse magnetic ($TM_0$) mode, the SPPs were effectively excited on the surface of the gold film [33, 34] at the tip of the probe and coupled to the m-SWCNTB, which propagated on the surface of the m-SWCNTB to the tip to achieve the compressive focusing of the optical field. Subsequently, we applied the dielectrophoresis method [35, 36] to assemble m-SWCNT into the fibre probe tip to fabricate the CNT-FP, and the scanning electron microscopy (SEM) characterization image is given in Fig. 1(c).

As a proof of concept, we set up a near-field optical measurement system and perform near-field optical testing of the light transmittance of a rectangular grating with a depth of 400 nm, a width of 400 nm using a conventional SPPs-FP and a CNT-FP, respectively. Finally, the quality of the near field optical image that measured by the CNT-FP, with the resolution of 72.1 nm, is more than 7 times better than conventional SPPs-FP.

**Validation of optical field focusing effect at the tip of CNT-FP.** In contrast to AFM probe composite carbon nanotubes, which are employed as CNT-FPs for near-field optical measurements, the formation of a focused light field necessitates the propagation of tip-excited SPPs to the m-SWCNTB tip. Therefore, we need to verify the coupling, propagation, and focusing effects of SPPs on the m-SWCNTB of the CNT-FP. We coupled the 633 nm wavelength laser into the CNT-FP, as shown in Fig. 2(a), and the scattered light field of the tip was observed with the side of an optical microscopy to verify the effect of m-SWCNTB at the tip of CNT-FP on the relaying of SPPs.

When SPPs are coupled from the gold film to the m-SWCNTB,

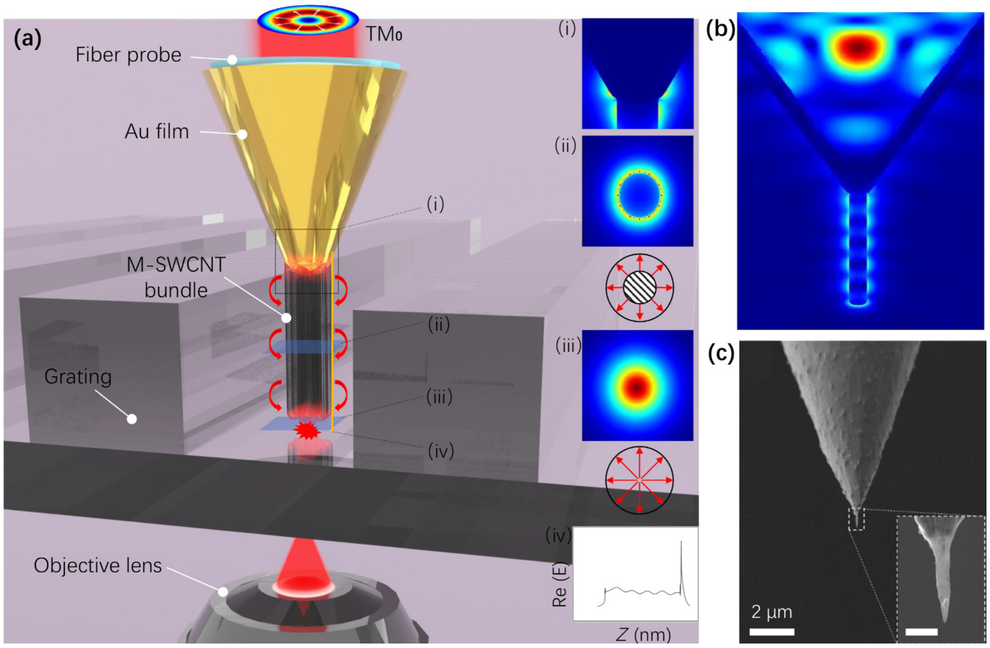


**Figure 1** Nano-focusing concepts of CNT-FP. (a) One-dimensional nanomaterial at the tip of the CNT-FP is a carbon nanotube bundle composed of multiple metallic carbon nanotubes, and the SPPs excited at the tip of the probe are coupled to the carbon nanotube bundle, shown in (i), and propagate to the tip to form a focused light field. (ii) The electric field distribution in the cross-section of SPPs as they propagate across the carbon nanotubes bundle. (iii) The focusing of the optical field at the tip of the carbon nanotube bundle. (iv) The distribution of electric field strength on the surface (depicted by the yellow line in the figure) in the direction of the carbon nanotube bundle axis as SPPs propagate along the carbon nanotube bundle. (b) Focusing simulation results of the propagation of SPPs in the tip region of the CNT-FP. (c) SEM characterisation of the CNT-FP, the scale of the small image is 150 nm.

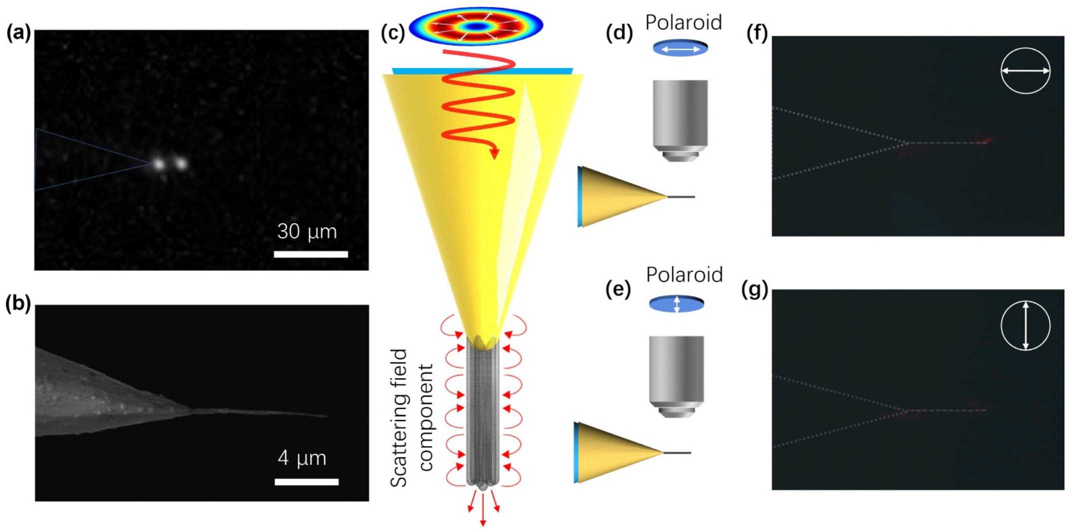


**Figure 2** Propagation and focusing verification of SPPs on the surface of the CNT-FP. (a) Scattered field at the tip of the CNT-FP, (b) SEM side-view characterization of the probe, (c) schematic of the scattered field distribution at the tip of the CNT-FP, the direction of the scattered field in the SPPs mode is perpendicular to the propagation interface. The scattered field is mainly distributed in the radial direction at the bond between the m-SWCNTB and the tip of the probe and distributed in the axial direction at the m-SWCNTB tip. (d) and (e) The observation of the scattered field at the tip of the probe through the polarizer in the axial direction and perpendicular to the axial direction. (f) and (g) The observation image through the polarizer of each other respectively, the grey dashed line in the vertical figure is the contour line of the tip of probe and the m-SWCNTB. The scattered field is mainly distributed along the vertical axis at the combination of the m-SWCNTB and the tip of the probe, and the scattered field is mainly distributed in the axial direction at the tip of the m-SWCNTB.

the angular and material mutations, in addition to the presence of defects at the junction, result in the scattering of some SPPs to the far field. This phenomenon can be observed through optical microscopy, as evidenced by the light spot on the left side in close proximity to the conical tip depicted in Fig. 2(b). SPPs propagate to the tip of the m-SWCNTB, thereby forming a focused light field that can be observed in the scattered field (Fig. 2(a), the light spot on the right side). In Fig. 2(a), two scattered light sources can be seen in the axial direction of the CNT-FP tip, and the distance between the two scattered light sources is consistent with the length of the m-SWCNTB in Fig. 2(b). It shows that SPPs successfully coupled to the m-SWCNTB and propagated to the m-SWCNTB tip. According to the propagation and electric field distribution characteristics of radially SPPs on the tapered tip and on the surface of cylindrical m-SWCNTB, the distribution characteristics of the optical field at the tip of carbon nanotubes can be investigated by the technique of far-field polarization analysis, i.e. the intensity distributions of the scattered or transmitted optical field at the tip of the probe are analyzed in far-field using a polarizer to demonstrate the nano-focusing of the SPPs modes at the tip of the probe. Figure 2(c) illustrates, with radially polarized light incidence, SPPs are excited at the tapered probe and propagate along the m-SWCNTB to the tip for focusing, and the components of its scattered field in different directions are constantly changing. The polarization component of the scattered light field is mainly distributed in the radial direction of m-SWCNTB during the propagation of the SPPs. As the SPPs propagate to the tip of the m-SWCNTB to produce a focused light field, the polarized component of the scattered light field is mainly distributed in the axial direction. Therefore, we analyzed the scattered light field at the side of the probe through polarizers as shown in Figs. 2(d) and 2(e), which are perpendicular and parallel, respectively, to the axis of the m-SWCNTB. In Figs. 2(f) and 2(g), it can be seen that the intensity of the scattered field perpendicular to the axial direction of the m-SWCNTB is greater than that in the axial direction at the point where the m-SWCNTB is bonded to the probe tip. The intensity of the scattered field in the axial direction at the tip of the m-SWCNTB is much larger than that in the perpendicular axial direction, which in turn proves that the SPPs have good propagation and focusing effects on the m-SWCNTB.

**CNT-FP/SPPs-FP comparison for nearfield optical measurement.** To verify the advantages of CNT-FP over conventional SPPs-FP in measuring the larger aspect ratio structure experiments, we set up a near-field optical measurement system and perform near-field optical testing of the light transmittance of a rectangular grating with the depth of 400 nm and the width of 400 nm using a conventional SPPs-FP and a CNT-FP, respectively.

As shown in Figs. 3(a) and 3(b), due to the geometrical limitation of the conventional SPPs-FP, the sidewalls of the probe will interfere with the structure to be measured during the measurement of the larger aspect ratio structure, thus affecting the movement stability of the probe and resulting in imaging distortion. In addition, the collection of near-field optical information necessitates that the distance between the tip of the probe and the sample be within the near-field range, is typically less than 20 nm. The tip does not enter the near-field range above the bottom surface of the sample, and the focused light field cannot interact with the bottom surface, thus failing to detect the bottom surface near-field optical information. That is why the vast majority of existing near-field optical measurement samples is comprised of quantum dots, nanowires, graphene, and other structures with a height approaching zero.

However, CNT-FP can be used to penetrate deep into the bottom of the larger aspect ratio structures with m-SWCNTB composited at the tip, the focused light field formed at the tip of the m-SWCNTB excites the near-field optical information at the base of the structure into the far-field for collection, enabling more precise measurements of near-field optical information. In order to verify the measurement capability of CNT-FP for measuring samples with larger aspect ratios, we chose a grating with a depth of

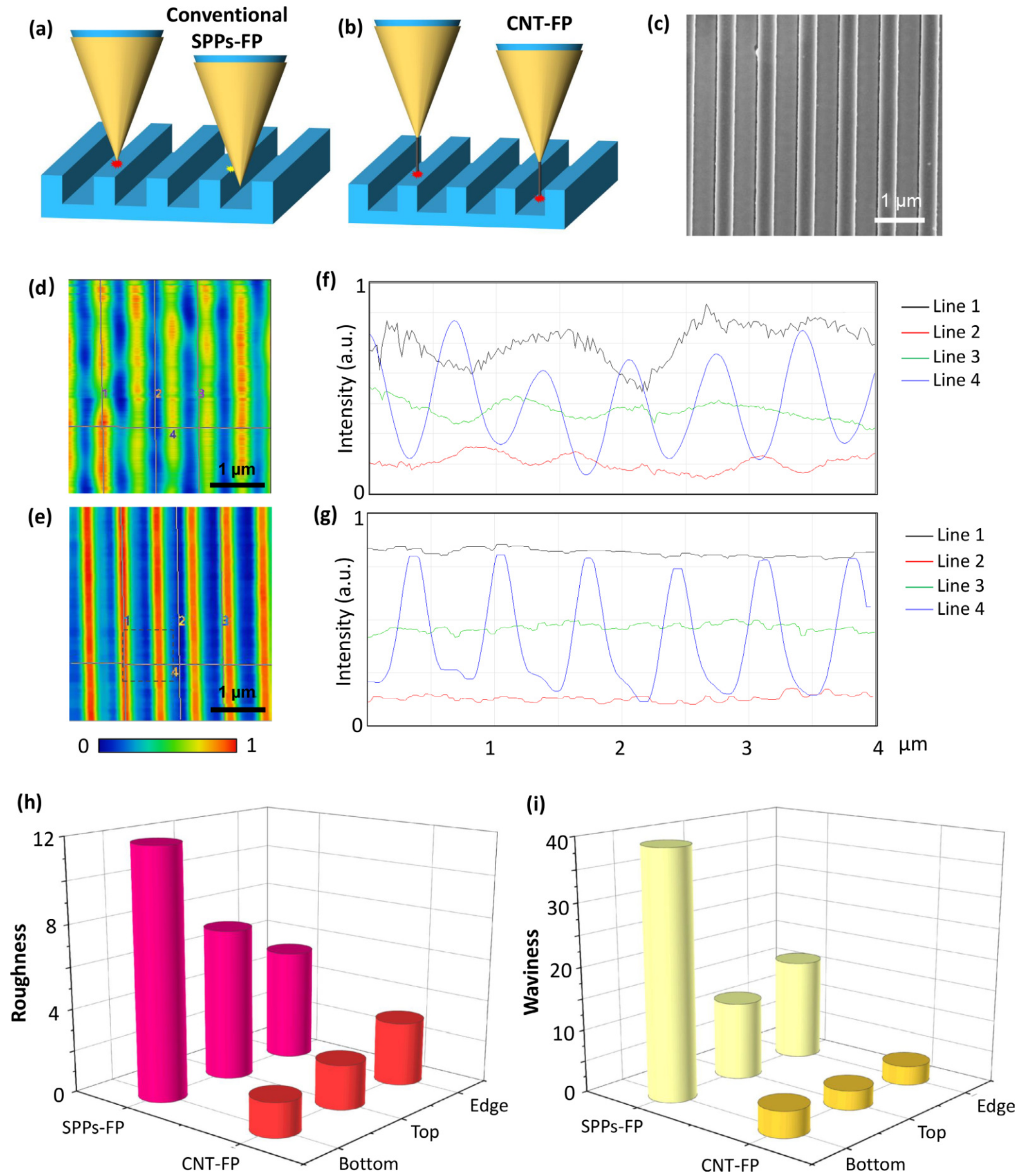


**Figure 3** CNT-FP testing. (a) and (b) The detailed plot comparison between a conventional SPPs-FP and a CNT-FP in the measurement of a grating with the aspect ratio. CNT-FP can penetrate deeper into the grating for more accurate scanning imaging than conventional SPPs-FP, which have geometric limitations that make it difficult to penetrate deeper into the grating. (c) SEM characterisation of the grating (covered with a layer of 20 nm Cr for conductivity). (d) and (e) The results of near-field optical tests of conventional SPPs-FP and CNT-FP, respectively. (f) and (g) The intensity distributions of the light field at the top, bottom, and side edge in the same direction as the grating and at four lines perpendicular to the direction of the grating selected in (c) and (d), respectively. (h) and (i) The comparison of roughness and waviness of the two probes at different positions along the grating direction, respectively.

400 nm and a section of 400 nm as a sample, as shown in Fig. 3(c). This sample is more than 100 times deeper in the vertical direction than traditional low-dimensional samples such as nanowires and graphene. To make the measurement effect of CNT-FP more intuitive, we simultaneously compare the measurement effect with that of conventional SPPs-FP. Figures 3(d) and 3(e) show the results of grating measurements for a width of 400 nm, a depth of 400 nm, and a period of 800 nm using a conventional SPPs-FP and a CNT-FP, respectively. It is evident that CNT-FP is a superior alternative to conventional SPPs-FP for near-field optical imaging of gratings with a large aspect ratio. Figures 3(f) and 3(g) show the light intensity distributions on three straight lines at the top, bottom, and side edge of the grating in the same direction as the extended grating and on a straight line perpendicular to the direction of the grating, selected from Figs. 3(d) and 3(e), respectively. As shown in the comparison diagram, the probe moves irregularly in the longitudinal direction of the image due to collision and interference between the probe side walls and the structure being inspected, resulting in image falsification when using the conventional SPPs-FP measurement. We use normalized average roughness and waviness to describe the stability of the measurements in the vertical direction.

As shown in Figs. 3(h) and 3(i), the imaging of line roughness of the measured light intensity signals at the bottom, top, and side edge of the grating for the conventional SPPs-FP are 11.84, 7.28, and 5.36, respectively, and the waviness are 39.18, 12.45, and 16.25, respectively. The imaging line roughness of the measured light intensity signals of the CNT-FP at the bottom, top, and side edge of the grating are 1.63, 2.13, and 3.04, respectively, and the waviness are 4.16, 3.09, and 3.11, respectively. From the above quantitative results, it can be seen that the CNT-FP is superior to the conventional SPPs-FP in terms of measurement stability and imaging quality, especially when measuring the light intensity information at the bottom of the grating, the normalized roughness and the waviness measured by the CNT-FP are better than those of the conventional SPPs-FP by factors of 7 and 9, respectively. In the transverse direction for imaging of rectangular grating transmitted light fields we used the variance of the normalized periodic extremum to evaluate the stability of the two probes in imaging of the grating transmitted light fields. The variances of the two extrema values of the period in the transverse direction for a conventional SPPs-FP are $1.46 \times 10^{-3}$ and $6.17 \times 10^{-4}$, respectively. While the values for CNT-FP are $4.41 \times 10^{-5}$ and $7.43 \times 10^{-5}$, respectively, which are much lower than the results measured by the conventional SPPs-FP, so the imaging stability measured by the CNT-FP is also better than that of the conventional SPPs-FP in the transverse direction.

Comparing the measurement images of the two probes, we can clearly see that, when measuring the bottom of the grating (light intensity maximum), there is a plateau in the signal measured by the CNT-FP, and we attribute this phenomenon to the near-field optical signal at the bottom of the grating measured by the smooth movement of the m-SWCNTB touching the bottom of the grating. The tip of the conventional SPPs-FP cannot reach the bottom of the grating structure, thus failing to obtain the near-field optical information of the bottom of the grating, and cannot present the platform-like light intensity signal. CNT-FP has better integrity for the detection of near-field optical information about the surface structure of samples when measuring samples with larger aspect ratios.

In addition, we selected the area with the size of 1 μm × 1 μm as shown in Fig. 4(a) at the rectangular box in Fig. 3(e) to verify the resolution of CNT-FP in measuring a large aspect ratio grating structure. The information of light intensity distribution along line 1 in Fig. 4(a) is illustrated in Fig. 4(b), and the half-height width is 72.1 nm. This level of resolution is comparable to the diameter size of the m-SWCNTB, as illustrated in Fig. 1(c). In contrast, the resolution capability demonstrated by conventional SPPs-FP in measurements of this grating sample with a large aspect ratio is only half the grating period, which is 400 nm. Consequently, CNT-FP offers superior resolution compared to conventional SPP-FP in measurements of intricate structures with larger aspect ratios. In order to verify the optical resolution of CNT-FP in measuring conventional nanostructures, we selected multi-walled carbon nanotubes as the sample. The measurement results are shown in Fig. 4(c). From the figure, we can see the shadows that are formed by the multi-walled bundles of carbon nanotubes in the transmission measurements. We chose two narrow slit shadows to determine the resolution limit of CNT-FP in the measurement of conventional nanostructures, as shown in Fig. 4(d). By measuring the half-height width of the peak light intensity, we can see that the resolution of the CNT-FP in measuring conventional nanostructures can break through 30 nm. And this resolution has reached the limit of the resolution of the transmission of the SNOM device used in this experiment.

**SPPs propagation evolution.** To further understand the coupling, propagation and focusing process of SPPs on the CNT-FP, we use a FDTD method to simulate the total process, and intuitively display the focusing effect of the light field on the CNT-FP tip. Firstly, as one-dimensional nanomaterials combined with fibre probes, it needs to have high SPPs propagation efficiency. The SPPs propagation characteristics on the surface of this one-dimensional nanomaterial can be obtained from solving the set of Maxwell's equations and boundary conditions for the one-dimensional nanomaterial-medium interface. In an infinite metallic material-dielectric three-dimensional interface, as shown in Fig. 4(a), the conditions for the propagation of SPPs on the surface of metallic objects should satisfy the electromagnetic wave boundary conditions. For the $TM_0$ mode, the electric field components are equal on both sides of the metal-dielectric interface in the direction of propagation, and the magnetic field components are equal on both sides of the interface in the transverse direction. Eventually we get the equation as follows

$$\frac{k_2}{k_1} = -\frac{\varepsilon_2}{\varepsilon_1} \tag{1}$$

where $k_1$ and $k_2$ denote the wave vector components perpendicular to the direction normal to the interface between the metal and the

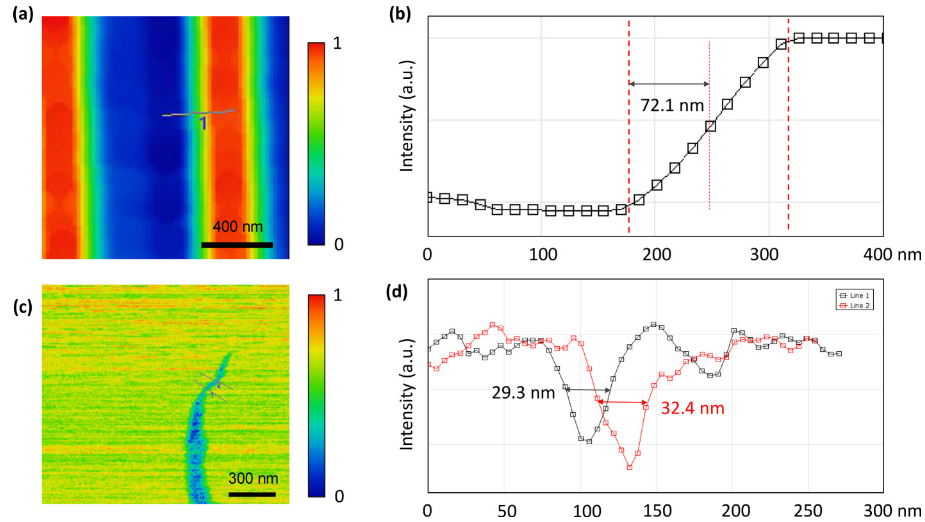


**Figure 4** CNT-FP resolution evaluation. (a) Detail image of the rectangular box in Fig. 3(d). (b) The intensity distribution of the light field at line 1 in (a). (c) Near-field optical imaging of multi-walled carbon nanotubes. (d) The intensity distribution of the light field at lines 1 and 2 in (c).

medium, respectively. $k_1$ and $k_2$ are positive real numbers, so the condition for the above equation to be valid is that $\varepsilon_1$ and $\varepsilon_2$ have opposite signs. Usually, the dielectric constant of the medium $\varepsilon_2$ is > 0, so the condition for the propagation of SPPs must be met $\mathrm{Re}(\varepsilon_1) < 0$. In the visible light to near-infrared band, the dielectric constants of metals and m-SWCNTs are usually less than zero. Therefore, m-SWCNTs can be used as one-dimensional nanomaterials for propagating SPPs in principle.

We bring in characteristic parameters such as the dielectric constant of m-SWCNTs and obtain the excitation, propagation, coupling, and focusing of the SPPs with the incidence of radially polarized light at a wavelength of 633 nm. Figure 5(a) shows the SPPs propagate along the m-SWCNTB to form a focus at the tip. Figure 5(b) shows the propagation of SPPs on the m-SWCNTB, and Fig. 5(c) shows the intensity distribution of the focused light field in the tip region of the m-SWCNTB, where the SPPs propagate to the tip of the m-SWCNTB to form a focused light field, which is shown in Fig. 5(d). The CNTB tip is positioned at a distance of approximately 20 nm from the sample using CNT-FP. At this proximity, the focused light field is enhanced between the tip and the sample. Figures 5(e)–5(g) show the effect of local electric field enhancement between the m-SWCNTB tip and the sample surface when the CNT-FP is used to measure $SiO_2$, Si, and Au samples, respectively. The difference in the intensity of the local enhanced electric field formed between the m-SWCNTB tip and the different materials can be used for imaging surfaces composed of different materials.

## 3 Conclusions

We proposed a CNT-FP to solve the difficulty of conventional SPPs-FP for accurate and high-quality near-field optical measurement imaging of samples with larger aspect ratios. We have verified the feasibility of propagation and focusing of SPPs on the m-SWCNTB of the CNT-FP tip. We prepared CNT-FPs and designed experiments for far-field polarization analysis. Propagation and focusing of the SPPs on the m-SWCNTB were verified by observation of the scattered light field. We finally used CNT-FP for near-field optical measurements of gratings with high aspect ratio and compared the results to those of conventional SPPs-FPs. The results of the measurements demonstrated that CNT-FP exhibited superior stability and accuracy in near-field optical imaging of larger aspect ratio gratings in comparison to conventional SPPs-FP. The evaluation indexes of waviness and line roughness demonstrate that CNT-FP exhibits a near-field optical imaging quality that is nearly an order of magnitude higher than that of conventional SPPs-FP. Furthermore, it has achieved a resolution of 72.1 nm measuring grating with larger aspect ratio. This approach was not limited to m-SWCNT, as well as materials such as Au nanowires and ZnO nanowires, can be employed in the assembly of composite fibre probes, which can then be utilized to achieve near-field optical measurements of large aspect ratio structures. Moreover, the new generation of microdevices and microsystems fabrication continues to push the limits of performance at the cost of the complexity of functionalized microstructures. For example, the angle of inclination of smooth surfaces of devices increases dramatically, and their functional structures evolve from single materials to multilayers with increasing trench depths. This study employs a combination of spectroscopic techniques that can be utilized for the detection of prospective semiconductor devices with intricate structures, as well as the characterization of complex biological structures.

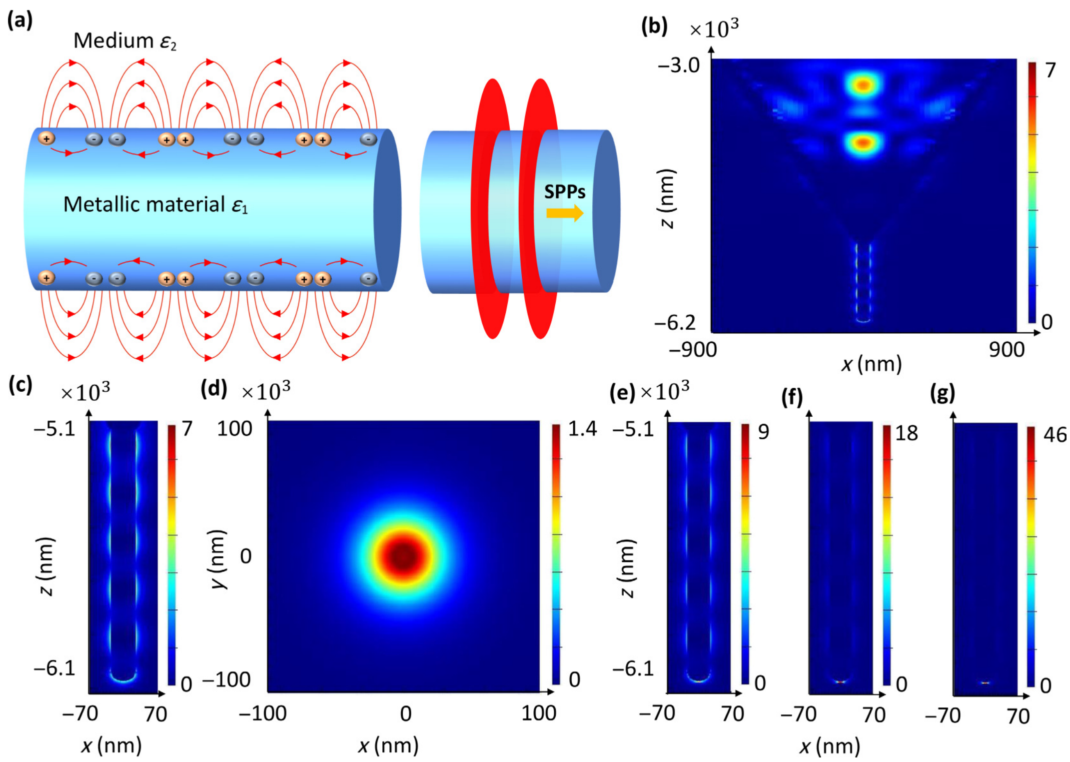


**Figure 5** FDTD simulation results of CNT-FP. (a) Schematic of SPPs propagation at the metallic material-dielectric interface. (b) Simulation of excitation and propagation of SPPs at the tip of the CNT-FP. (c) Focusing process of SPPs propagation in m-SWCNTB. (d) Focusing effect of optical field at the tip of m-SWCNTB. (e)–(g) Focusing effect of light field between CNT-FP and $SiO_2$, Si, Au samples.

## 4 Materials and methods

**Preparation of fibre probes.** A 633 nm laser light source was chosen for the experiment, and to ensure that the optical fibre could propagate the $TM_0$ mode light, we chosed a 780HP single mode optical fibre as the material for preparing the optical fibre probe. The optical fibre was immersed in 40% hydrofluoric acid for 2 h and 55 min to obtain a tip with a radius of curvature of tens of nanometres. An 80 nm thick gold film was then deposited uniformly on the surface of the tip using magnetron ion sputtering to obtain a fibre-optic probe that can be used for near-field optical detection.

**M-CNTs dispersant preparation.** We used the 99% pure metallic carbon nanotubes produced by NanoIntegris, with a single diameter of 1.2–1.7 nm and a length of 300–5000 nm. The stock solution was prepared at a concentration of 0.01 wt.%, which was subsequently diluted 200-fold to yield a solution of 0.00005 wt.% with anhydrous ethanol. The diluted metallic carbon nanotube dispersion was subjected to ultrasound treatment for a period of 24 h, resulting in the formation of the m-CNT dispersion, which was subsequently employed in the preparation of CNT-FPs.

**Manufactured CNT-FP with dielectrophoresis method.** As shown in Figs. S1 and S2 in the Electronic Supplementary Material (ESM), the function signal generator produces a sinusoidal AC signal voltage with a frequency of 1 MHz and a voltage of 20 VPP, and the positive and negative poles of the signal line are connected to the fibre probe with gold-plated film and the electrode plate, respectively, to generate an AC electric field between the tip of the probe and the electrode plate. The free CNT in the CNT dispersion moved towards the tip of the probe under the action of dielectrophoretic force, and arranged in the direction of the electric field line at the tip of the probe to form a SWCNTB.

**Modified CNT-FP with focused ion beam (FIB).** FIB was used to modify the CNT bundle at the tip of the CNT-FP. Following the assembly of the CNT-FP using dielectrophoresis, the length of the SWCNTB at its front end was observed to range from a few micrometres to a dozen micrometres. As shown in Fig. S3 in the ESM, it was demonstrated that the CNT-FP of a specific length can be selected for modification according to the structure of the sample under test. The use of longer carbon nanotube bundles would result in more pronounced tailing effects during the measurement process. Therefore, it is recommended that shorter carbon nanotube bundles be employed wherever possible to ensure optimal imaging results in accordance with the aspect ratio and the dimensions of the sample to be measured.

**Measurement by SNOM.** The experiments were performed in tuning fork shear mode on a NSOM module (NT-MDT), which integrated an inverted optical microscopy and a photomultiplier tube for light intensity acquisition. The light source was a laser with the wavelength of 633 nm coupled to the fibre tail through an objective lens.

**Electronic Supplementary Material**: Supplementary material (CNT-FP preparation technology and process) is available in the online version of this article at https://doi.org/10.26599/NR.2025.94907254.

## Data availability

All data needed to support the conclusions in the paper are presented in the manuscript and the Electronic Supplementary Material. Additional data related to this paper may be requested from the corresponding author upon request.

## Acknowledgements

The authors would like to acknowledge the support by the National Science Fund for Outstanding Young Scholars (No. 52225507).

## Declaration of competing interest

All the contributing authors report no conflict of interests in this work.

## Author contribution statement

W. H. T.: Writing manuscript, experiments, and analysis. S. H. Z., H. J. D., Z. Z., P. R. J., S. H. Q., and W. B. H.: Experiments and analysis. J. L. Z., R. J. Z.: Discussions. S. M. Y. and corresponding author: Conception, experimental design, discussions, manuscript modification. All the authors have approved the final manuscript.

## Use of AI statement

None.

## References

[1] Krug, J. T.; Sánchez, E. J.; Xie, X. S. Design of near-field optical probes with optimal field enhancement by finite difference time domain electromagnetic simulation. *J. Chem. Phys.* **2002**, *116*, 10895–10901.

[2] Giugni, A.; Torre, B.; Toma, A.; Francardi, M.; Malerba, M.; Alabastri, A.; Zaccaria, R. P.; Stockman, M. I.; Di Fabrizio, E. Hot-electron nanoscopy using adiabatic compression of surface plasmons. *Nat. Nanotechnol.* **2013**, *8*, 845–852.

[3] Tugchin, B. N.; Janunts, N.; Klein, A. E.; Steinert, M.; Fasold, S.; Diziain, S.; Sison, M.; Kley, E. B.; Tünnermann, A.; Pertsch, T. Plasmonic tip based on excitation of radially polarized conical surface plasmon polariton for detecting longitudinal and transversal fields. *ACS Photonics* **2015**, *2*, 1468–1475.

[4] Wang, F.; Li, S. B.; Zhao, S. H.; Zhang, Z.; Ji, P. R.; Xia, C. S.; Cheng, B. Y.; Zhang, G. F.; Yang, S. M. A flat-based plasmonic fiber probe for nanoimaging. *Nano Res.* **2023**, *16*, 7545–7549.

[5] Minn, K.; Birmingham, B.; Ko, B.; Ko, B.; Lee, H. W. H.; Lee, H. W. H.; Lee, H. W. H.; Lee, H. W. H.; Lee, H. W. H.; Zhang, Z. R. et al. Interfacing photonic crystal fiber with a metallic nanoantenna for enhanced light nanofocusing. *Photonics Res.* **2021**, *9*, 252–258.

[6] Choi, S. S.; Park, M. J.; Han, C. H.; Oh, S. J.; Han, S. H.; Park, N. K.; Kim, Y. S.; Choo, H. Fabrication of pyramidal probes with various periodic patterns and a single nanopore. *J. Vac. Sci. Technol. B* **2015**, *33*, 06F203.

[7] Hou, Y. P.; Ma, C. F.; Wang, W. T.; Chen, Y. H. A dual-use probe for nano-metric photoelectric characterization using a confined light field generated by photonic crystals in the cantilever. *Nano Res.* **2021**, *14*, 3848–3853.

[8] Ropers, C.; Neacsu, C. C.; Elsaesser, T.; Albrecht, M.; Raschke, M. B.; Lienau, C. Grating-coupling of surface plasmons onto metallic tips: A nanoconfined light source. *Nano Lett.* **2007**, *7*, 2784–2788.

[9] Zhang, Z.; Ahn, P.; Dong, B. Q.; Balogun, O.; Sun, C. Quantitative imaging of rapidly decaying evanescent fields using plasmonic near-field scanning optical microscopy. *Sci. Rep.* **2013**, *3*, 2803.

[10] Tuniz, A.; Chemnitz, M.; Dellith, J.; Weidlich, S.; Schmidt, M. A. Hybrid-mode-assisted long-distance excitation of short-range surface plasmons in a nanotip-enhanced step-index fiber. *Nano Lett.* **2017**, *17*, 631–637.

[11] Kim, S.; Yu, N.; Ma, X. Z.; Zhu, Y. Z.; Liu, Q. S.; Liu, M.; Yan, R. X. High external-efficiency nanofocusing for lens-free near-field optical nanoscopy. *Nat. Photonics* **2019**, *13*, 636–643.

[12] Zhang, R.; Zhang, Y.; Dong, Z. C.; Jiang, S.; Zhang, C.; Chen, L. G.; Zhang, L.; Liao, Y.; Aizpurua, J.; Luo, Y. et al. Chemical mapping of a single molecule by plasmon-enhanced Raman scattering. *Nature* **2013**, *498*, 82–86.

[13] Xu, D.; Xiong, X.; Wu, L.; Ren, X. F.; Png, C. E.; Guo, G. C.; Gong, Q. H.; Xiao, Y. F. Quantum plasmonics: New opportunity in fundamental and applied photonics. *Adv. Opt. Photonics* **2018**, *10*, 703–756.

[14] Németh, G.; Datz, D.; Tóháti, H. M.; Pekker, Á.; Kamarás, K. Scattering near-field optical microscopy on metallic and semiconducting carbon nanotube bundles in the infrared. *Phys. Status Solidi B* **2016**, *253*, 2413–2416.

[15] Zhang, W. H.; Fu, Y. Y.; Li, H. J.; Gu, Z. N.; Zhang, Z. H.; Zhu, X. Discrete polarization absorption property of carbon nanotubes studied by using scanning near-field optical microscope. *Scanning* **2004**, *26*, I21–I25.

[16] Beitner, D.; Amitay, S.; Atrt, S. S.; Richter, S.; Suchowski, H.; Ben Shalom, M. S-SNOM imaging of stacking order in few-layer graphene. In 2023 Conference on Lasers and Electro-Optics Europe & European Quantum Electronics Conference, Munich, Germany, 2023; IEEE, p 1.

[17] Wirth, K. G.; Linnenbank, H.; Steinle, T.; Banszerus, L.; Icking, E.; Stampfer, C.; Giessen, H.; Taubner, T. Tunable s-SNOM for nanoscale infrared optical measurement of electronic properties of bilayer graphene. *ACS Photonics* **2021**, *8*, 418–423.

[18] Gadelha, A. C.; Ohlberg, D. A. A.; Rabelo, C.; Neto, E. G. S.; Vasconcelos, T. L.; Campos, J. L.; Lemos, J. S.; Ornelas, V.; Miranda, D.; Nadas, R. et al. Localization of lattice dynamics in low-angle twisted bilayer graphene. *Nature* **2021**, *590*, 405–409.

[19] Kim, P.; Adorno-Martinez, W. E.; Khan, M.; Aizenberg, J. Enriching libraries of high-aspect-ratio micro- or nanostructures by rapid, low-cost, benchtop nanofabrication. *Nat. Protoc.* **2012**, *7*, 311–327.

[20] Chang, H. K.; Kim, Y. K. UV-LIGA process for high aspect ratio structure using stress barrier and C-shaped etch hole. *Sens. Actuators A: Phys.* **2000**, *84*, 342–350.

[21] Paek, J.; Kim, J. Microsphere-assisted fabrication of high aspect-ratio elastomeric micropillars and waveguides. *Nat. Commun.* **2014**, *5*, 3324.

[22] Slattery, A. D.; Shearer, C. J.; Gibson, C. T.; Shapter, J. G.; Lewis, D. A.; Stapleton, A. J. Carbon nanotube modified probes for stable and high sensitivity conductive atomic force microscopy. *Nanotechnology* **2016**, *27*, 475708.

[23] Chin, S. C.; Chang, Y. C.; Chang, C. S. The fabrication of carbon nanotube probes utilizing ultra-high vacuum transmission electron microscopy. *Nanotechnology* **2009**, *20*, 285307.

[24] Cheng, B. Y.; Yang, S. M.; Li, W.; Li, S.; Shafique, S.; Wu, D.; Ji, S. Y.; Sun, Y.; Jiang, Z. D. Controlled growth of a single carbon nanotube on an AFM probe. *Microsyst. Nanoeng.* **2021**, *7*, 80.

[25] Guo, X.; Qiu, M.; Bao, J. M.; Wiley, B. J.; Yang, Q.; Zhang, X. N.; Ma, Y. G.; Yu, H. K.; Tong, L. M. Direct coupling of plasmonic and photonic nanowires for hybrid nanophotonic components and circuits. *Nano Lett.* **2009**, *9*, 4515–4519.

[26] Ma, X. Z.; Zhu, Y. Z.; Yu, N.; Kim, S.; Liu, Q. S.; Apontti, L.; Xu, D.; Yan, R. X.; Liu, M. Toward high-contrast atomic force microscopy-tip-enhanced Raman spectroscopy imaging: Nanoantenna-mediated remote-excitation on sharp-tip silver nanowire probes. *Nano Lett.* **2019**, *19*, 100–107.

[27] Fujita, Y.; Walke, P.; De Feyter, S.; Uji-I, H. Remote excitation-tip-enhanced Raman scattering microscopy using silver nanowire. *Jpn. J. Appl. Phys.* **2016**, *55*, 08NB03.

[28] Dai, H. J.; Javey, A.; Pop, E.; Mann, D.; Kim, W.; Lu, Y. R. Electrical transport properties and field effect transistors of carbon nanotubes. *Nano* **2006**, *1*, 1–13.

[29] Poncharal, P.; Berger, C.; Yi, Y.; Wang, Z. L.; de Heer, W. A. Room temperature ballistic conduction in carbon nanotubes. *J. Phys. Chem. B* **2002**, *106*, 12104–12118.

[30] Lu, W.; Xiong, Y.; Chen, L. W. Length-dependent dielectric polarization in metallic single-walled carbon nanotubes. *J. Phys. Chem. C* **2009**, *113*, 10337–10340.

[31] Rathinavel, S.; Priyadharshini, K.; Panda, D. A review on carbon nanotube: An overview of synthesis, properties, functionalization, characterization, and the application. *Mater. Sci. Eng.: B* **2021**, *268*, 115095.

[32] Suri, A.; Coleman, K. S. The superiority of air oxidation over liquid-phase oxidative treatment in the purification of carbon nanotubes. *Carbon* **2011**, *49*, 3031–3038.

[33] Lu, F. F.; Zhang, W. D.; Zhang, L.; Liu, M.; Xue, T. Y.; Huang, L. G.; Gao, F.; Mei, T. Nanofocusing of surface plasmon polaritons on metal-coated fiber tip under internal excitation of radial vector beam. *Plasmonics* **2019**, *14*, 1593–1599.

[34] Li, S. B.; Yang, S. M.; Wang, F.; Liu, Q.; Cheng, B. Y.; Rosenwaks, Y. Plasmonic interference modulation for broadband nanofocusing. *Nanophotonics* **2021**, *10*, 4113–4123.

[35] Abdulhameed, A.; Halim, M. M.; Halin, I. A. Dielectrophoretic alignment of carbon nanotubes: Theory, applications, and future. *Nanotechnology* **2023**, *34*, 242001.

[36] Stokes, P.; Khondaker, S. I. High quality solution processed carbon nanotube transistors assembled by dielectrophoresis. *Appl. Phys. Lett.* **2010**, *96*, 083110.